From Space to Earth – Relative-CoM-to-Foot (RCF) control yields high contact robustness

Johannes Englsberger, Alessandro M. Giordano, Achraf Hiddane, Robert Schuller, Florian Loeffl, George Mesesan, Christian Ott

***Abstract*— This paper introduces the Simplest Articulated Free-Floating (SAFF) model, a low-dimensional model facilitating the examination of controllers, which are designed for free-floating robots that are subject to gravity. Two different state-of-the-art control approaches, namely absolute CoM control accompanied by an assumption about the foot acceleration, and a controller combining absolute CoM and foot control objectives, are shown to yield exponential stability in the nominal case, while becoming unstable if the foot contact is lost. As an improvement over the state of the art, the so-called Relative-CoM-to-Foot (RCF) controller is introduced, which again yields exponential stability nominally, while preserving a BIBO stable behavior even in case of a complete contact loss. The controller performance is validated in various simulations.**

I. Introduction

The control of free-floating robots, whether in space or on earth, is an exciting field of research. One of the biggest challenges with regard to such robots is their intrinsic under-actuation: According to Newton's second law, their centroidal dynamics, which includes both angular momentum and linear momentum (the latter being directly related to the robot's Center of Mass (CoM) dynamics), may under certain circumstances be completely uncontrollable, e.g. in space, or conditionally controllable, e.g. on earth.

This paper takes inspiration from the field of space robotics. The dynamics modeling w.r.t. the CoM was introduced in [1]. So-called barycentric vectors were exploited for modeling in [2]. A first step towards the use of relative quantities in control was taken in [3], where the so-called generalized Jacobian was introduced to control the end-effector of a space robot assuming zero linear and angular momenta. In [4]–[6], the generalized Jacobian-related *internal* and *circumcentroidal* velocities of a frame were defined and used for end effector control without excitation of the CoM. The velocities correspond to the relative CoM-to-end-effector velocity measured in rotating and non-rotating centroidal frames, respectively.

As compared to space-related applications, the control of free-floating robots on earth has a more recent past. Until today, many humanoid and other legged robots are position-controlled [7]–[9]. Due to their rigidity, they have to be carefully controlled when interacting with unstructured environments, e.g. while walking. While keeping balance of the overall system is a challenge, an instability of joint postures is very unlikely, because the latter are directly commanded by the controls or planning algorithm, and strictly followed. In contrast, torque-controllable robots such as [10], [11] have the advantage of an intrinsically more compliant interaction with their environment. However, in comparison to position control, torque-based whole-body controllers (WBC) have much more feedback channels, torque-based position control is only achieved indirectly and stability cannot always be guaranteed. Henze et al. [12] achieved passivity-based balancing on compliant ground surfaces with the humanoid robot TORO [10], while Mesesan et al. [13] made the same robot walk over compliant mattresses and gravel. Bellicoso et al. [14] perform various dynamic gaits with the quadruped ANYmal [15] by optimizing the whole-body motion and contact forces. Fahmi et al. introduced STANCE [16], a quadratic programming (QP) based soft terrain adaptation algorithm. STANCE allows for locomotion over multiple terrains of different compliances and is able to withstand external perturbations. However, it cannot handle cases of complete contact loss.

This paper newly introduces the so-called Relative-CoM-to-Foot (RCF) controller. It is based on the insight that the relative CoM-to-foot dynamics is always controllable, while the absolute CoM dynamics, i.e. with respect to the inertial frame, is only conditionally controllable. RCF control is stable both during stance and during flight (or a free

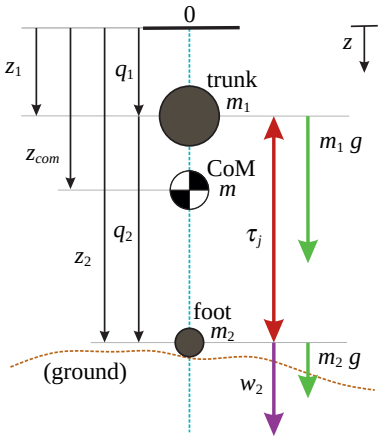

Fig. 1: Simplest Articulated Free-Floating (SAFF) model: two links (trunk, foot) that are constrained to move vertically; subject to gravity; one actuated joint between trunk and foot ($\rightarrow \tau_j$); foot may potentially apply force w_2 towards ground.

The authors are with Institute of Robotics and Mechatronics, German Aerospace Center (DLR), 82234 Wessling, Germany. E-mail: johannes.englsberger@dlr.de

fall), and thus can be used without switching. In case of appropriate foot constraints, i.e. ground contact, this relative controller can be anyhow used for absolute CoM tracking control, since the constraints cause a concordance of relative and absolute CoM coordinates. This is due to the fact that controlling the CoM w.r.t. the world is kind of equivalent to controlling it w.r.t. its world-fixed foot. In case of unstable contact, e.g. when slipping or stepping into a hollow, RCF control guarantees postural stability, thereby increasing the likelihood of an eventual recovery after ground contact has been re-established. To the best of our knowledge, RCF is the first heuristic-free, purely torque-based whole-body controller (WBC) that is robust to severe contact imperfections, while the state of the art (e.g. [17]–[23]) is either not robust w.r.t. this issue, or uses heuristics that are hard to predict and cannot guarantee stability.

The paper is organized as follows: Section II introduces the low-dimensional model used throughout the paper, while Sec. III recapitulates our previous work on Modular Passive Tracking Control (MPTC). Sections IV and V introduce the considered tasks and derive different controllers, respectively. In Sec. VI, simulation results are presented. Section VII provides a discussion, while Sec. VIII concludes the paper.

II. Equation of Motion and Constraint Forces

A. Simplest Articulated Free-Floating (SAFF) model

In this work, we propose the Simplest Articulated Free-Floating (SAFF) model (see Fig. 1). It consists of two point-masses (m_1 and m_2 representing the trunk and the foot, respectively) and one actuated joint between them (the corresponding joint torque τ_j denotes here a linear force). The foot may potentially[1] be in contact with the ground and be subject to a contact / foot force w_2.

1) Kinematics: The SAFF model is based on two *generalized coordinates* q_1 and q_2, collected in the generalized coordinate vector $\boldsymbol{q} = [q_1, q_2]^T$, where q_1 corresponds to the trunk position and q_2 is the relative coordinate between trunk and foot. The *absolute coordinates* z_1 and z_2 of the trunk and foot, respectively, are collected as

$$\boldsymbol{z} \;=\; \begin{bmatrix} z_1 \\ z_2 \end{bmatrix} \;=\; \underbrace{\begin{bmatrix} 1 & 0 \\ 1 & 1 \end{bmatrix}}_{\boldsymbol{J}} \boldsymbol{q} \;. \tag{1}$$

Note that due to the linearity of the SAFF model, the forward kinematics map $\boldsymbol{J}$ is equivalent to the corresponding Jacobian matrix. Also note that the downward direction is defined as *positive*. The absolute trunk velocity $\dot{z}_1$ and foot velocity $\dot{z}_2$ are

$$\dot{z}_1 \;=\; \underbrace{\begin{bmatrix} 1 & 0 \end{bmatrix}}_{\boldsymbol{J}_1} \dot{\boldsymbol{q}} \qquad \text{and} \qquad \dot{z}_2 \;=\; \underbrace{\begin{bmatrix} 1 & 1 \end{bmatrix}}_{\boldsymbol{J}_2} \dot{\boldsymbol{q}} \;. \tag{2}$$

The robot's Center of Mass (CoM) can be computed as

$$z_{com} \;=\; \frac{m_1}{m}\, z_1 \;+\; \frac{m_2}{m}\, z_2 \;, \tag{3}$$

where $m = m_1 + m_2$ denotes the total robot mass. The CoM velocity can be computed as

$$\dot{z}_{com} \;=\; \begin{bmatrix} \frac{m_1}{m} & \frac{m_2}{m} \end{bmatrix} \boldsymbol{J}\, \dot{\boldsymbol{q}} \;=\; \underbrace{\begin{bmatrix} 1 & \frac{m_2}{m} \end{bmatrix}}_{\boldsymbol{J}_{com}} \dot{\boldsymbol{q}} \;. \tag{4}$$

2) Dynamics: Applying the balance of forces (see Fig. 1), we find the trunk and foot dynamics to be

$$m_1\, \ddot{z}_1 \;=\; m_1\, g \;-\; \tau_j \qquad \text{and} \qquad m_2\, \ddot{z}_2 \;=\; m_2\, g \;+\; \tau_j \;+\; w_2 \;. \tag{5}$$

The CoM dynamics is

$$m\, \ddot{z}_{com} \;=\; m_1\, \ddot{z}_1 \;+\; m_2\, \ddot{z}_2 \;=\; m\, g \;+\; w_2 \;. \tag{6}$$

Collecting the CoM and foot dynamics in matrix form yields

$$\begin{bmatrix} m & 0 \\ 0 & m_2 \end{bmatrix} \begin{bmatrix} \ddot{z}_{com} \\ \ddot{z}_2 \end{bmatrix} \;+\; \begin{bmatrix} -mg \\ -m_2 g \end{bmatrix} \;=\; \begin{bmatrix} 0 \\ 1 \end{bmatrix} \tau_j \;+\; \begin{bmatrix} 1 \\ 1 \end{bmatrix} w_2 \;. \tag{7}$$

Expressing the absolute CoM and foot acceleration as a function of generalized accelerations $\ddot{\boldsymbol{q}}$, namely

$$\begin{bmatrix} \ddot{z}_{com} \\ \ddot{z}_2 \end{bmatrix} \;=\; \begin{bmatrix} J_{com} \\ J_2 \end{bmatrix} \ddot{\boldsymbol{q}} \;=\; \begin{bmatrix} 1 & \frac{m_2}{m} \\ 1 & 1 \end{bmatrix} \ddot{\boldsymbol{q}} \;, \tag{8}$$

equation (7) can be rewritten as

$$\underbrace{\begin{bmatrix} m & m_2 \\ m_2 & m_2 \end{bmatrix}}_{\boldsymbol{M}} \ddot{\boldsymbol{q}} \;+\; \underbrace{\begin{bmatrix} -m\, g \\ -m_2\, g \end{bmatrix}}_{\tau_g = -\boldsymbol{J}_{com}^T\, m\, g} \;=\; \underbrace{\begin{bmatrix} 0 \\ 1 \end{bmatrix}}_{\boldsymbol{S}^T} \tau_j \;+\; \underbrace{\begin{bmatrix} 1 \\ 1 \end{bmatrix}}_{\boldsymbol{J}_2^T} w_2 \;, \tag{9}$$

which is the *equation of motion* of the SAFF model. The right hand side of (9) can be interpreted as the generalized torques

$$\boldsymbol{\tau} \;=\; \underbrace{\begin{bmatrix} \boldsymbol{S}^T & \boldsymbol{J}_2^T \end{bmatrix}}_{\boldsymbol{U}} \underbrace{\begin{bmatrix} \tau_j \\ w_2 \end{bmatrix}}_{\boldsymbol{u}} \;=\; \underbrace{\begin{bmatrix} 0 & 1 \\ 1 & 1 \end{bmatrix}}_{\boldsymbol{U}} \boldsymbol{u} \;. \tag{10}$$

Note that (9) has precisely the form of the general free-floating robot equation of motion[2] (EoM, see e.g. [24], [25]):

$$\boldsymbol{M}\, \ddot{\boldsymbol{q}} \;+\; \boldsymbol{C}\, \dot{\boldsymbol{q}} \;+\; \boldsymbol{\tau}_g \;=\; \underbrace{\boldsymbol{S}^T \boldsymbol{\tau}_j \;+\; \boldsymbol{J}_c^T \boldsymbol{w}_c}_{\boldsymbol{\tau}} \;, \tag{11}$$

where $\boldsymbol{J}_c$ and w_c are the stacks of contact Jacobians and wrenches, respectively, relating to links in contact with the environment. Note that in (9) $\boldsymbol{C} = \boldsymbol{0}$ since $\boldsymbol{M}$ is constant.

B. Actual and estimated constraint force

This section provides the actual and estimated constraint force, for the case that the foot is in contact with the ground. This is typically modeled by imposing a constraint on the foot acceleration $\ddot{z}_2$. Solving (5, right) for w_2, we find

$$w_2 = m_2(\ddot{z}_2 - g) - \tau_j \;, \tag{12}$$

which returns the foot force w_2, in case the joint torque τ_j and the foot acceleration $\ddot{z}_2$ are known.

Equation (12) can be applied to estimate the foot force $w_{2,est}$, given the commanded joint torque $\tau_{j,cmd}$ and an estimate of the foot acceleration $\ddot{z}_{2,est}$:

$$w_{2,est} = m_2(\ddot{z}_{2,est} - g) - \tau_{j,cmd} \tag{13}$$

[1] This paper examines several controllers regarding their contact robustness. Accordingly, we consider the case of firm foot contact with the ground, and the case for which the foot is completely free, i.e. there is no ground.

[2] Note: the dependencies of the matrices on $\boldsymbol{q}$ and $\dot{\boldsymbol{q}}$ are omitted here.

III. Recapitulation of our previous publication on Modular Passive Tracking Control (MPTC)

In our previous work [25], we proposed the Modular Passive Tracking Control (MPTC), which is a generic control framework, serving as template for arbitrary specific controllers, e.g. Cartesian or joint controllers. For the SAFF model (see Fig. 1) with its lack of Coriolis terms, MPTC results in the same control law as an Inverse Dynamics controller (see section IV-A in [25]). Nevertheless, we recapitulate some of the most relevant equations from [25], since they facilitate the analysis of different controllers, especially with regard to passivity. Also, we intend to apply MPTC theory when extending the Relative-CoM-to-Foot (RCF) controller that will be presented in Sec. V-C to full 3D robot models, e.g. humanoids, motivating the short summary here.

In [25], we proposed to use one *separate Lyapunov function* based on the task-related relative kinetic energy $E_{kin,k}$ and relative potential energy $E_{pot,k}$ for each one of the n_T tasks:

$$V_k = \underbrace{\frac{1}{2}\,\dot{\tilde{\boldsymbol{x}}}_k^T\,\boldsymbol{M}_k\,\dot{\tilde{\boldsymbol{x}}}_k}_{E_{kin,k}} + \underbrace{\frac{1}{2}\,\tilde{\boldsymbol{x}}_k^T\,\boldsymbol{K}_k\,\tilde{\boldsymbol{x}}_k}_{E_{pot,k}} \quad , \tag{14}$$

where the positive definite, symmetric matrix $\boldsymbol{K}_k$ denotes the task stiffness, and $\boldsymbol{M}_k$ is the task inertia (see [25] for details). This Lyapunov function is positive definite in the task position error $\tilde{\boldsymbol{x}}_k$ and the task velocity error $\dot{\tilde{\boldsymbol{x}}}_k = \dot{\boldsymbol{x}}_{k,ref} - \underbrace{\boldsymbol{J}_k\,\dot{\boldsymbol{q}}}_{\dot{\boldsymbol{x}}_k}$, with $\boldsymbol{J}_k$ denoting the task Jacobian. Accordingly, we defined the (actual) *task force*[3] $\boldsymbol{f}_k$ as:

$$\boldsymbol{f}_k = \underbrace{\boldsymbol{M}_k\,\boldsymbol{J}_k\,\boldsymbol{M}^{-1}}_{\boldsymbol{T}_k^T}\,\boldsymbol{\tau} \quad , \tag{15}$$

where $\boldsymbol{T}_k$ denotes the dynamically consistent pseudo-inverse of $\boldsymbol{J}_k^T$. By choosing the *desired task force* $\boldsymbol{f}_{k,des}$ as

$$\boldsymbol{f}_{k,des} = \boldsymbol{T}_k\boldsymbol{\tau}_g + \boldsymbol{M}_k\,\boldsymbol{Q}_k\,\dot{\boldsymbol{q}} + \boldsymbol{M}_k\,\ddot{\boldsymbol{x}}_{k,ref} + (\boldsymbol{C}_k + \boldsymbol{D}_k)\,\dot{\tilde{\boldsymbol{x}}}_k + \boldsymbol{K}_k\,\tilde{\boldsymbol{x}}_k \;, \tag{16}$$

where $\boldsymbol{C}_k$ is the task Coriolis matrix, $\boldsymbol{Q}_k$ is another Coriolis related matrix and $\boldsymbol{D}_k$ is a positive definite damping matrix, the time derivative of (14) is brought into the following form:

$$\dot{V}_k = \underbrace{-\dot{\tilde{\boldsymbol{x}}}_k^T\,\boldsymbol{D}_k\,\dot{\tilde{\boldsymbol{x}}}_k}_{\dot{V}_{k,des},\ \text{purely dissipative}} + \underbrace{\dot{\tilde{\boldsymbol{x}}}_k^T\,\tilde{\boldsymbol{f}}_k}_{\dot{\tilde{V}}_k} \;, \tag{17}$$

where $\tilde{\boldsymbol{f}}_k = \boldsymbol{f}_{k,des} - \boldsymbol{f}_k$. Accordingly, the task error dynamics becomes

$$\boldsymbol{M}_k\,\ddot{\tilde{\boldsymbol{x}}}_k + \Big(\boldsymbol{C}_k + \boldsymbol{D}_k\Big)\,\dot{\tilde{\boldsymbol{x}}}_k + \boldsymbol{K}_k\,\tilde{\boldsymbol{x}}_k = \tilde{\boldsymbol{f}}_k \;. \tag{18}$$

It is important to note that (17) yields perfect dissipation of task errors and (18) yields an asymptotically converging, compliant task behavior *only if* the corresponding task force error $\tilde{\boldsymbol{f}}_k$ is zero. Thus, (17) and (18) have to be interpreted as representations of the task-related overall system energies and dynamics from the perspective of the task objectives (16), until an actual controller is inserted through (15) by setting the joint torque to the commanded one, i.e. $\tau_j = \tau_{j,cmd}$.

[3]Note: depending on the task, the task force may contain linear forces, torques, wrenches, etc.

IV. Overview of considered tasks

In this section, we introduce three different tasks, namely:

- a CoM task that is defined w.r.t. the inertial frame,
- a foot task that is defined w.r.t. the inertial frame, and
- a relative CoM-vs-foot task.

Note: Each controller presented in Sec. V implements a subset of these tasks.

A. CoM task (w.r.t. inertial frame)

Applying (16), we find the desired CoM task force as

$$\begin{aligned} f_{com,des} &= \boldsymbol{T}_{com}\,\boldsymbol{\tau}_g + m\,\ddot{z}_{com,ref} + d_{com}\,\dot{\tilde{z}}_{com} + k_{com}\,\tilde{z}_{com} \\ &= m\,(\ddot{z}_{com,ref} - g) + d_{com}\,\dot{\tilde{z}}_{com} + k_{com}\,\tilde{z}_{com} \;, \end{aligned} \tag{19}$$

where $m_{com} = (\boldsymbol{J}_{com}\boldsymbol{M}^{-1}\boldsymbol{J}_{com}^T)^{-1} = m$, $\boldsymbol{Q}_{com} = \boldsymbol{C}_{com} = \boldsymbol{0}$, $\boldsymbol{T}_{com} = m\,\boldsymbol{J}_{com}\,\boldsymbol{M}^{-1} = [1,0]$, and d_{com} and k_{com} denote the CoM damping and stiffness. Applying (15) and (10) yields

$$f_{com} = \boldsymbol{T}_{com}\,\boldsymbol{\tau} = \underbrace{\boldsymbol{T}_{com}\,\boldsymbol{U}}_{\boldsymbol{T}_{U,com}}\underbrace{\begin{bmatrix}\tau_j\\ w_2\end{bmatrix}}_{\boldsymbol{u}} = \underbrace{[0,1]}_{\boldsymbol{T}_{U,com}}\begin{bmatrix}\tau_j\\ w_2\end{bmatrix} = w_2 \;. \tag{20}$$

Similarly, applying (17) and (18) to the CoM task yields the (absolute) CoM Lyapunov rate

$$\begin{aligned} \dot{V}_{com} &= -d_{com}\,\dot{\tilde{z}}_{com}^2 + \dot{\tilde{z}}_{com}\,(f_{com,des} - f_{com}) \\ &= \dot{\tilde{z}}_{com}\Big(m\,(\ddot{z}_{com,ref} - g) + k_{com}\,\tilde{z}_{com} - w_2\Big) \;, \end{aligned} \tag{21}$$

and the (absolute) CoM error dynamics

$$m\,\ddot{\tilde{z}}_{com} + d_{com}\,\dot{\tilde{z}}_{com} + k_{com}\,\tilde{z}_{com} = f_{com,des} - f_{com} \;, \tag{22}$$

respectively.

B. Foot task (w.r.t. inertial frame)

As for the CoM, we apply (16) to the foot task to obtain

$$\begin{aligned} f_{2,des} &= \boldsymbol{T}_2\,\boldsymbol{\tau}_g + m_2\,\ddot{z}_{2,ref} + d_2\,\dot{\tilde{z}}_2 + k_2\,\tilde{z}_2 \\ &= m_2\,(\ddot{z}_{2,ref} - g) + d_2\,\dot{\tilde{z}}_2 + k_2\,\tilde{z}_2 \;, \end{aligned} \tag{23}$$

where $m_2 = (\boldsymbol{J}_2\boldsymbol{M}^{-1}\boldsymbol{J}_2^T)^{-1}$, $\boldsymbol{T}_2 = m_2\boldsymbol{J}_2\boldsymbol{M}^{-1} = [0,1]$, $\boldsymbol{Q}_2 = \boldsymbol{C}_2 = \boldsymbol{0}$, and d_2 and k_2 denote the foot damping and stiffness gains. Again, applying (15) and (10) yields

$$f_2 = \boldsymbol{T}_2\,\boldsymbol{\tau} = \underbrace{\boldsymbol{T}_2\,\boldsymbol{U}}_{\boldsymbol{T}_{U,2}}\underbrace{\begin{bmatrix}\tau_j\\ w_2\end{bmatrix}}_{\boldsymbol{u}} = \underbrace{[1,1]}_{\boldsymbol{T}_{U,2}}\begin{bmatrix}\tau_j\\ w_2\end{bmatrix} = \tau_j + w_2 \tag{24}$$

Similarly, applying (17) and (18) to the foot task yields the (absolute) foot Lyapunov rate

$$\begin{aligned} \dot{V}_2 &= -d_2\,\dot{\tilde{z}}_2^2 + \dot{\tilde{z}}_2\,(f_{2,des} - f_2) \\ &= \dot{\tilde{z}}_2\Big(m_2\,(\ddot{z}_{2,ref} - g) + k_2\,\tilde{z}_2 - \tau_j - w_2\Big) \;, \end{aligned} \tag{25}$$

and the (absolute) foot error dynamics

$$m_2\,\ddot{\tilde{z}}_2 + d_2\,\dot{\tilde{z}}_2 + k_2\,\tilde{z}_2 = f_{2,des} - f_2 \;, \tag{26}$$

respectively.

C. Relative CoM-to-foot task

Now, in addition to the previously introduced *absolute* CoM and foot tasks, we define a *relative* CoM-to-foot task, which is based on the relative task coordinate

$$z_R = z_{com} - z_2 \ . \tag{27}$$

The corresponding task velocity can be computed as

$$\dot{z}_R = \dot{z}_{com} - \dot{z}_2 = (\boldsymbol{J}_{com} - \boldsymbol{J}_2)\,\dot{\boldsymbol{q}} = \underbrace{\left[0, -\frac{m_1}{m}\right]}_{\boldsymbol{J}_R}\,\dot{\boldsymbol{q}} \ . \tag{28}$$

The task Jacobian $\boldsymbol{J}_R$ is used to compute the task inertia

$$m_R = \left(\boldsymbol{J}_R\,\boldsymbol{M}^{-1}\,\boldsymbol{J}_R^T\right)^{-1} = \frac{m_2\,m}{m_1} \ , \tag{29}$$

and the task mapping matrix

$$\boldsymbol{T}_R = m_R\,\boldsymbol{J}_R\,\boldsymbol{M}^{-1} = \left[\frac{m_2}{m_1}, -\frac{m}{m_1}\right] \ . \tag{30}$$

Applying (16) we find the desired task force

$$f_{R,des} = m_R\,\ddot{z}_{R,ref} + d_R\,\dot{\tilde{z}}_R + k_R\,\tilde{z}_R \ , \tag{31}$$

where $\tilde{z}_R = z_{R,ref} - z_R$ and $\dot{\tilde{z}}_R = \dot{z}_{R,ref} - \dot{z}_R$ denote the relative position and velocity errors, respectively. Interestingly, in contrast to (19) and (23), the term $\boldsymbol{T}_R\,\boldsymbol{\tau}_g = 0$ cancels. As for the other tasks, $\boldsymbol{Q}_R = \boldsymbol{C}_R = \boldsymbol{0}$, making (31) a particularly simple controller objective. Using (15) and (10), we find the actual relative CoM-to-foot task force as:

$$f_R = \boldsymbol{T}_R \underbrace{\boldsymbol{U}\,\boldsymbol{u}}_{\boldsymbol{\tau}} = \underbrace{\left[-\frac{m}{m_1}, -1\right]}_{\boldsymbol{T}_{U,R}} \underbrace{\begin{bmatrix}\tau_j \\ w_2\end{bmatrix}}_{\boldsymbol{u}} = -\frac{m}{m_1}\,\tau_j - w_2 \ . \tag{32}$$

Applying (17) and (18) to the CoM-vs-foot task yields the corresponding Lyapunov rate

$$\begin{aligned}\dot{V}_R &= -d_R\,\dot{\tilde{z}}_R^2 + \dot{\tilde{z}}_R\,(\underbrace{f_{R,des} - f_R}_{\tilde{f}_R}) \qquad (33)\\ &= \dot{\tilde{z}}_R\left(m_R\,\ddot{z}_{R,ref} + k_R\,\tilde{z}_R + \underbrace{\frac{m}{m_1}\,\tau_j + w_2}_{-f_R}\right) \ ,\end{aligned}$$

and the task error dynamics

$$m_R\,\ddot{\tilde{z}}_R + d_R\,\dot{\tilde{z}}_R + k_R\,\tilde{z}_R = \underbrace{f_{R,des} - f_R}_{\tilde{f}_R} \ . \tag{34}$$

Finally, inserting (31) into (34) yields

$$m_R\,\ddot{z}_R = \underbrace{-\frac{m}{m_1}\,\tau_j - w_2}_{f_R} \ . \tag{35}$$

Again note that (35) is not a function of gravity.

V. Derivation and Robustness Analysis of Different Controller Setups

In this section, we will present three different controllers: two controllers from the literature and the newly proposed one. Each of them is examined regarding its stability properties and robustness against contact imperfections. In particular, two extreme contact scenarios are considered: a fully constrained foot motion (considering zero foot acceleration, i.e. $\ddot{z}_2 = 0$), and a completely free foot (i.e. foot force $w_2 = 0$).

A. Absolute CoM task with foot acceleration assumption

In this subsection, we derive a controller that tracks *absolute* CoM trajectories (i.e. in world frame), while being based on an *assumption / estimate* for the foot acceleration, typically $\ddot{z}_{2,est} = 0$. This type of controller has been widely used in research [20]–[23] and can be seen as the state of the art in humanoid and bipedal whole-body control (WBC). It comes, however, with two disadvantages:

- It is likely to become unstable in case of imperfect foot contact conditions (see Sec. V-A.3).
- It requires a switching of controllers when transitioning from stance to swing and/or back.

The latter leads to high sensitivity regarding timing issues, leading to an increased effort for ensuring safe and continuous transitions between the different controller modes.

1) Controller derivation: In (20), we replace τ_j by the estimated joint torque $\tau_{j,est} = \tau_{j,cmd}$, and w_2 by $w_{2,est}$ from (13), which yields the estimated absolute CoM task force

$$\begin{aligned}f_{com,est} &= \boldsymbol{T}_{U,com}\begin{bmatrix}\tau_{j,est}\\ w_{2,est}\end{bmatrix} = \begin{bmatrix}0,1\end{bmatrix}\begin{bmatrix}\tau_{j,cmd}\\ m_2\,(\ddot{z}_{2,est} - g) - \tau_{j,cmd}\end{bmatrix}\\ &= m_2\,(\ddot{z}_{2,est} - g) - \tau_{j,cmd} \ . \qquad (36)\end{aligned}$$

Now, setting $f_{com,est} = f_{com,des}$ from (19) and solving for the commanded joint torque $\tau_{j,cmd}$ yields the control law

$$\boxed{\tau_{j,cmd} = m_1\,g + m_2\,\ddot{z}_{2,est} - m\,\ddot{z}_{com,ref} - d_{com}\dot{\tilde{z}}_{com} - k_{com}\tilde{z}_{com} \ .} \tag{37}$$

Note that the Lyapunov rate from (21) and the absolute CoM task error dynamics from (22) are primarily independent from the joint torque τ_j, as long as w_2 remains unspecified.

2) Control performance for fully constrained foot motion: In case of a fully constrained foot, the foot acceleration is zero, i.e. $\ddot{z}_2 = 0$. Here, we also assume that the estimated foot acceleration is zero, i.e. $\ddot{z}_{2,est} = 0$. For this case and additionally inserting $\tau_j = \tau_{j,cmd}$, (12) becomes

$$\underbrace{w_2}_{f_{com}} = \underbrace{m\,(\ddot{z}_{com,ref} - g) + d_{com}\,\dot{\tilde{z}}_{com} + k_{com}\,\tilde{z}_{com}}_{f_{com,des}} \ , \tag{38}$$

i.e. the desired CoM task force is perfectly achieved. Inserting (38) into (21) and (22) yields the *contact-constrained absolute CoM task Lyapunov rate*

$$\dot{V}_{com} = -d_{com}\,\dot{\tilde{z}}_{com}^2 \ , \tag{39}$$

and the *contact-constrained absolute CoM error dynamics*

$$m_{com}\,\ddot{\tilde{z}}_{com} + d_{com}\,\dot{\tilde{z}}_{com} + k_{com}\,\tilde{z}_{com} = 0 \ , \tag{40}$$

which reveals that the absolute CoM controller is exponentially stable in the fully constrained case.

3) Control performance for completely unconstrained foot: If the robot's foot looses contact to the ground completely (e.g. when stepping into a deep hollow), it is fully unconstrained, such that $w_2 = 0$, and equation (21) becomes

$$\dot{V}_{com} = \dot{\tilde{z}}_{com}\left(m\,(\ddot{z}_{com,ref} - g) + k_{com}\,\tilde{z}_{com}\right) \ , \tag{41}$$

while (22) turns into $\ddot{z}_{com} = g$, i.e. the CoM accelerates downwards, following its natural falling dynamics.

B. Absolute CoM task and additional foot control

This subsection examines the controller presented in [25] that works with an absolute CoM controller *and* an absolute foot controller (both defined w.r.t. the inertial frame).

1) Controller derivation: Collecting the desired absolute CoM and foot task forces from (19) and (23) yields

$$\underbrace{\begin{bmatrix} f_{com,des} \\ f_{2,des} \end{bmatrix}}_{\boldsymbol{f}_{des}} = \begin{bmatrix} m\,(\ddot{z}_{com,ref} - g) + d_{com}\,\dot{\tilde{z}}_{com} + k_{com}\,\tilde{z}_{com} \\ m_2\,(\ddot{z}_{2,ref} - g) + d_2\,\dot{\tilde{z}}_2 + k_2\,\tilde{z}_2 \end{bmatrix} \quad . \tag{42}$$

Applying (20) and (24) to the controller commands, we find

$$\underbrace{\begin{bmatrix} f_{com,cmd} \\ f_{2,cmd} \end{bmatrix}}_{\boldsymbol{f}_{cmd}} = \underbrace{\begin{bmatrix} \boldsymbol{T}_{U,com} \\ \boldsymbol{T}_{U,2} \end{bmatrix}}_{\boldsymbol{T}_U} \begin{bmatrix} \tau_{j,cmd} \\ w_{2,cmd} \end{bmatrix} = \underbrace{\begin{bmatrix} 0 & 1 \\ 1 & 1 \end{bmatrix}}_{\boldsymbol{T}_U} \underbrace{\begin{bmatrix} \tau_{j,cmd} \\ w_{2,cmd} \end{bmatrix}}_{\boldsymbol{u}_{cmd}} \quad . \tag{43}$$

Obviously, $\boldsymbol{T}_U$ is invertible. We can set $\boldsymbol{f}_{cmd} = \boldsymbol{f}_{des}$ and solve for the commanded control input $\boldsymbol{u}_{cmd}$. Its elements are

$$\boxed{\begin{aligned} \tau_{j,cmd} \;=\; & m_1(g - \ddot{z}_{com,ref}) + m_2(\ddot{z}_{2,ref} - \ddot{z}_{com,ref}) \\ & - d_{com}\,\dot{\tilde{z}}_{com} - k_{com}\,\tilde{z}_{com} + d_2\,\dot{\tilde{z}}_2 + k_2\,\tilde{z}_2 \;, \end{aligned}} \tag{44}$$

and

$$w_{2,cmd} \;=\; m\,(\ddot{z}_{com,ref} - g) \;+\; d_{com}\,\dot{\tilde{z}}_{com} \;+\; k_{com}\,\tilde{z}_{com} \quad . \tag{45}$$

While the actual controller consists of (44), i.e. of the commanded joint torques $\tau_{j,cmd}$, the commanded foot force (45) can be seen as *pseudo-control input*. Basically, the controller assumes to have a thruster in the foot, which is obviously wrong and may lead to controller imperfections (e.g. regarding tracking performance, see Table I). The *actual foot force* w_2 cannot be controlled directly, but only via the commanded joint torques in combination with *correctly estimated* foot constraints. The motivation of using this pseudo-control in [25] was to keep the foot controllers *activated and unmodified* at all times, i.e. throughout stance and swing phases, avoiding a switching of controllers. Despite the mentioned imperfections, this facilitated the implementation of a WBC that enabled TORO [10] to walk in experiments with low tuning effort (see [25]). However, in case of foot positioning errors, we observed CoM and posture deviations.

In the following, we examine the behavior of controller (44) assuming an ideal torque source, i.e. $\tau_j = \tau_{j,cmd}$. Note that the CoM Lyapunov rate (21) and CoM dynamics (6) are not affected by τ_j and thus neither by $\tau_{j,cmd}$, as long as w_2 is considered to be generic, i.e. (possibly) independent from the joint torques τ_j. In contrast, the foot Lyapunov rate (25) and foot error dynamics (26) are functions of the joint torque τ_j, and, through setting $\tau_j = \tau_{j,cmd}$, turn into

$$\dot{V}_2 = -d_2\,\dot{\tilde{z}}_2^2 \;+\; \dot{\tilde{z}}_2\,(\underbrace{m\,(\ddot{z}_{com,ref} - g) + d_{com}\dot{\tilde{z}}_{com} + k_{com}\tilde{z}_{com}}_{f_{com,des} = w_{2,cmd}} - w_2) \;, \tag{46}$$

and

$$m_2\ddot{\tilde{z}}_2 + d_2\dot{\tilde{z}}_2 + k_2\tilde{z}_2 = \underbrace{m\,(\ddot{z}_{com,ref} - g) + d_{com}\dot{\tilde{z}}_{com} + k_{com}\tilde{z}_{com}}_{f_{com,des} = w_{2,cmd}} - w_2 \;. \tag{47}$$

2) Control performance for fully constrained foot motion: If the foot is constrained to not accelerate, i.e. $\ddot{z}_2 = 0$, and if the joint torque $\tau_j = \tau_{j,cmd}$, equation (12) turns into

$$\begin{aligned} w_2 \;=\; & \underbrace{m\,(\ddot{z}_{com,ref} - g) \;+\; d_{com}\,\dot{\tilde{z}}_{com} \;+\; k_{com}\,\tilde{z}_{com}}_{w_{2,cmd}} \\ & - (\underbrace{m_2\,\ddot{z}_{2,ref} \;+\; d_2\,\dot{\tilde{z}}_2 \;+\; k_2\,\tilde{z}_2}_{\Delta w_2}) \;. \end{aligned} \tag{48}$$

Now, with this particular foot force w_2, (21) turns into

$$\dot{V}_{com} \;=\; \underbrace{-d_{com}\,\dot{\tilde{z}}_{com}^2}_{\dot{V}_{com,des}} + \dot{\tilde{z}}_{com}\,(\underbrace{m_2\,\ddot{z}_{2,ref} \;+\; d_2\,\dot{\tilde{z}}_2 \;+\; k_2\,\tilde{z}_2}_{\Delta w_2}) \;, \tag{49}$$

while the error CoM dynamics (22) becomes

$$m\,\ddot{\tilde{z}}_{com} + d_{com}\,\dot{\tilde{z}}_{com} + k_{com}\,\tilde{z}_{com} = \underbrace{m_2\,\ddot{z}_{2,ref} + d_2\,\dot{\tilde{z}}_2 + k_2\,\tilde{z}_2}_{\Delta w_2} \;. \tag{50}$$

Assuming a bounded foot force error Δw_2 as input, this CoM dynamics is bounded-input-boundet-output (BIBO) stable. For this controller setup, the CoM dynamics is perturbed by the foot tracking errors (i.e. the right hand side of (50)). The latter may e.g. be caused by disturbances or unexpected ground heights (planned foot position below/above actual ground).

Note: in a fully static case, i.e. for $\dot{z}_{com} = \dot{z}_{com,ref} = \ddot{z}_{com} = \ddot{z}_{com,ref} = \dot{z}_2 = \dot{z}_{2,ref} = \ddot{z}_2 = \ddot{z}_{2,ref} = 0$, the CoM error is directly proportional to the foot placement error:

$$\tilde{z}_{com} \;=\; \frac{k_2}{k_{com}}\,\tilde{z}_2 \;. \tag{51}$$

Also note that since the foot is considered to be fully constrained here, there is no need to explicitly examine the corresponding Lyapunov rate and task error dynamics.

3) Control performance for completely unconstrained foot: For a complete foot contact loss ($w_2 = 0$), (6) becomes

$$\ddot{z}_{com} \;=\; g \;, \tag{52}$$

which shows that the CoM simply accelerates downward[4] due to gravity. In that case, (21), (46) and (47) become

$$\dot{V}_{com} \;=\; \dot{\tilde{z}}_{com}\left(m\,(\ddot{z}_{com,ref} \;-\; g) \;+\; k_{com}\,\tilde{z}_{com}\right) \;, \tag{53}$$

$$\dot{V}_2 \;=\; -d_2\,\dot{\tilde{z}}_2^2 \;+\; \dot{\tilde{z}}_2\,(\underbrace{m\,(\ddot{z}_{com,ref} - g) \;+\; d_{com}\,\dot{\tilde{z}}_{com} \;+\; k_{com}\,\tilde{z}_{com}}_{f_{com,des} = w_{2,cmd}}) \;, \tag{54}$$

and

$$m_2\,\ddot{\tilde{z}}_2 + d_2\,\dot{\tilde{z}}_2 + k_2\,\tilde{z}_2 = \underbrace{m\,(\ddot{z}_{com,ref} - g) + d_{com}\,\dot{\tilde{z}}_{com} + k_{com}\,\tilde{z}_{com}}_{f_{com,des} = w_{2,cmd}} \;, \tag{55}$$

respectively. While the left side of (55) is BIBO stable, the right side is unbounded due to the infinitly growing CoM position and velocity errors, making the system unstable.

[4]The positive sign here results from the convention of a downward pointing z-coordinate axis in Fig. 1.

	controllers		
	absolute CoM control + foot accel. assumpt. (Sec. V-A)	absolute CoM + foot control (Sec. V-B)	relative CoM-vs-foot control (Sec. V-C)
precise trajectory tracking for nominal contact conditions	✓	(✓)	✓
single controller supports swing and stance (no switching)	✗	✓	✓ (future research)
robust to ground loss	✗	✗	✓

TABLE I: Overview of features of the different examined controllers.

Note however: if (and only if) the damping and stiffness gains are chosen as $d_2 = d_{com}$ and $k_2 = k_{com}$, respectively, this controller becomes equivalent to RCF control presented in the next section, and thus the system is BIBO stable.

C. Relative-CoM-to-Foot (RCF) controller with foot acceleration assumption

This subsection finally introduces our proposed controller setup that stands out due to its high contact robustness. It combines the advantages of the two controllers from sections V-A and V-B. These are

- *precise CoM trajectory tracking* in case of well-established foot contact
- the possibility of using *one single relative CoM-to-foot controller* during different contact phases, facilitating implementation and improving robustness.

Additionally, in contrast to the other two controllers, it is robust to severe contact imperfections, including a complete loss of foot contact.

1) Controller derivation: In (32), we replace τ_j by the estimated joint torque $\tau_{j,est} = \tau_{j,cmd}$, and w_2 by $w_{2,est}$ from (13), which yields the estimated relative task force

$$\begin{aligned} f_{R,est} &= \boldsymbol{T}_{U,R} \begin{bmatrix} \tau_{j,est} \\ w_{2,est} \end{bmatrix} = \left[-\frac{m}{m_1}, -1 \right] \begin{bmatrix} \tau_{j,cmd} \\ m_2 \left(\ddot{z}_{2,est} - g \right) - \tau_{j,cmd} \end{bmatrix} \\ &= -m_2 \left(\ddot{z}_{2,est} - g \right) - \frac{m_2}{m_1} \tau_{j,cmd} \ . \end{aligned} \tag{56}$$

Now, setting $f_{R,est} = f_{R,des}$ from (31), and solving for the commanded joint torque $\tau_{j,cmd}$ yields the control law

$$\boxed{\tau_{j,cmd} = -m_1 \left(\ddot{z}_{2,est} - g \right) - m \, \ddot{z}_{R,ref} - \frac{m_1}{m_2} d_R \, \dot{\tilde{z}}_R - \frac{m_1}{m_2} k_R \, \tilde{z}_R \ .} \tag{57}$$

Now, we first insert the controller (57) into the Lyapunov rate from (33) and the relative task dynamics from (34), while leaving w_2 unspecified. Given a perfect joint torque source, i.e. $\tau_j = \tau_{j,cmd}$, this yields the following Lyapunov rate

$$\dot{V}_R = \dot{\tilde{z}}_R \left(-\frac{m}{m_2} d_R \, \dot{\tilde{z}}_R - \frac{m_1}{m_2} k_R \, \tilde{z}_R + m \left(g - \ddot{z}_{2,est} - \ddot{z}_{R,ref} \right) + w_2 \right) \tag{58}$$

and the following relative task error dynamics

$$m_R \, \ddot{\tilde{z}}_R + \frac{m}{m_2} d_R \, \dot{\tilde{z}}_R + \frac{m}{m_2} k_R \, \tilde{z}_R = w_2 + m \left(g - \ddot{z}_{2,est} - \ddot{z}_{R,ref} \right) . \tag{59}$$

2) Control performance for fully constrained foot motion: The acceleration of a fully constrained foot is zero, i.e. $\ddot{z}_2 = 0$. Here, we will also assume that the estimated foot acceleration is zero, i.e. $\ddot{z}_{2,est} = 0$. For this case and additionally inserting $\tau_j = \tau_{j,cmd}$, the foot force from (12) becomes

$$w_2 = m \left(\ddot{z}_{R,ref} - g \right) + \frac{m_1}{m_2} d_R \, \dot{\tilde{z}}_R + \frac{m_1}{m_2} k_R \, \tilde{z}_R \ . \tag{60}$$

Inserting (60) into (58) and (59) yields the *contact-constrained relative task Lyapunov rate*

$$\dot{V}_R = -d_R \, \dot{\tilde{z}}_R^2 \tag{61}$$

and the *contact-constrained relative task error dynamics*

$$m_R \, \ddot{\tilde{z}}_R + d_R \, \dot{\tilde{z}}_R + k_R \, \tilde{z}_R = 0 \ , \tag{62}$$

revealing that the Relative-CoM-to-Foot (RCF) controller is exponentially stable in the fully constrained case.

3) Control performance for completely unconstrained foot: If the robot's foot looses contact to the ground completely, it is fully unconstrained, such that $w_2 = 0$. If the foot acceleration is *estimated* to be $\ddot{z}_{2,est} = 0$, (58) turns into

$$\dot{V}_R = \dot{\tilde{z}}_R \left(m \left(g - \ddot{z}_{R,ref} \right) - \frac{m}{m_2} d_R \, \dot{\tilde{z}}_R - \frac{m_1}{m_2} k_R \, \tilde{z}_R \right) \ , \tag{63}$$

and the relative CoM-to-foot error dynamics (59) becomes

$$m_R \, \ddot{\tilde{z}}_R + \frac{m}{m_2} d_R \, \dot{\tilde{z}}_R + \frac{m}{m_2} k_R \, \tilde{z}_R = \underbrace{m \left(g - \ddot{z}_{R,ref} \right)}_{\text{bounded}} \ , \tag{64}$$

which is BIBO stable for the input $m \left(g - \ddot{z}_{R,ref} \right)$.

For the regulation case (i.e. $\dot{z}_{R,ref} = \ddot{z}_{R,ref} = 0$), the system is asymptotically stable, but the relative coordinate converges to $z_R = z_{R,ref} - \frac{m_2 \, g}{k_R}$, corresponding to an over-stretching of the leg relative to the CoM. This can also be observed in Fig. 2 (center plot) during the fall. The Lyapunov rate (63) may become positive especially right after the contact loss due to the gravity over-compensation and the corresponding leg over-stretching. However, another Lyapunov function can be designed, for which the error dynamics (64) can be shown to be passive.

Another interesting observation is the following: One can show that for a stiffness and damping design that results in two equal negative eigenvalues (and thus critical damping) for the nominal error dynamics (62), also the resulting eigenvalues of the free-falling error dynamics (64) are real and negative, resulting in a straight convergence during fall, rather than an excessive oscillatory behavior.

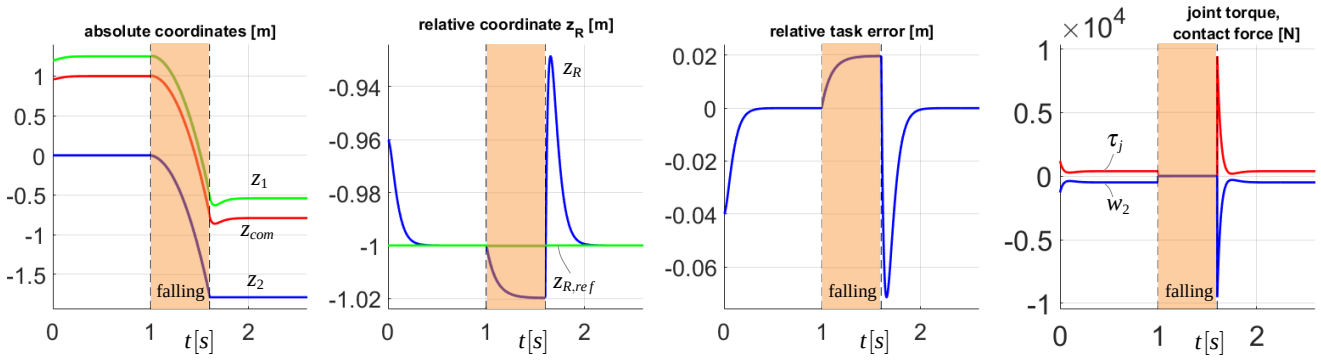

Fig. 2: Standing-falling-standing scenario: for $z_{R,ref} = \text{const.} = 1m$.

VI. Simulation Results

In a first simulation, the robot ($m_1 = 40kg$, $m_2 = 10kg$) tries to stabilize a stationary relative reference pose between the CoM and the foot (corresponding to $z_R = 1m$). After an initial convergence from a random starting condition, the ground breaks away at $t = 1.0s$ and the robot falls for 0.6s and about 1.8m deep. Afterwards, the foot re-establishes ground contact. During the fall, the relative coordinate z_R, i.e. the distance between the CoM and the foot, grows for the proposed RCF controller. Since the controller does not know that the contact is lost, it still tries to compensate for gravity. However, the corresponding pushing force is quickly and continuously compensated by the growing impedance force, such that a new equilibrium[5] is reached. After the impact, the controller quickly converges back to the setpoint (see Fig. 2). In contrast, both controllers from the state of the art (sections (V-A) and (V-B)) become unstable[6] right after the loss of contact for a comparable simulation.

In a further simulation we used the exact same setup as in the first one, however, imposing a sinusoidal reference trajectory for the relative coordinate z_R. Again, the RCF controller shows perfect tracking performance in case of firm ground contact, while a safely bounded tracking error is observed during the fall (see Fig. 3).

VII. Insights, Discussion and Future Research

The main insight of the paper is the following: The absolute CoM dynamics is only guaranteed to be controllable, if the assumptions made about the foot contact situation at hand (e.g. zero foot acceleration) hold true, i.e. it is only *conditionally controllable*. The truly controllable quantity is the *relative CoM-to-foot dynamics* (or similar quantities), and this regardless of the contact situation. The Relative-CoM-to-Foot (RCF) controller presented in Sec. V-C yields precise tracking if the foot dynamics is naturally constrained (zero foot acceleration). In a free fall situation, it proves to be BIBO stable. We speculate that our claims regarding BIBO stability can be generalized to any foot contact scenario (e.g. contact of foot with compliant terrain, slipping, etc.). A corresponding in-depth analysis is part of our future research. It is, however, also important to note that our proposed RCF controller partially leaves aside the problem of the possibly uncontrollable CoM dynamics, which becomes most obvious in case of a free falling scenario: While the relative CoM-to-foot dynamics is stable and behaves well, the CoM itself, lacking any means of counteraction, is subject to gravity and thus follows a free-fall. This means, the absolute CoM dynamics is unstable in that case. However, especially with regard to an eventual recovery in case of a timely landing on a lower ground level (see accompanying video), the natural stability of the RCF controller can be seen as an important advantage over other controllers: it preserves the robot's posture rather than becoming unstable.

In this paper, we assume that the foot constraint force is the only external force acting on the system. In case of external disturbances (pushes etc.), the presented Lyapunov rates and task error dynamics would have additional perturbation terms. We believe that the latter do not have an impact on passivity, while an impedance / compliance behavior would take the place of the nominally exponential stability (if applicable in the unperturbed case). The detailed examination of such effects is also part of our future research.

VIII. Conclusion

In this paper, we introduced the Simplest Articulated Free-Floating (SAFF) model, which due to its low complexity and dimensionality facilitates the examination of free-floating robot controllers. We could show that two different control approaches, namely absolute CoM control accompanied by an assumption about the foot acceleration (state of the art) and a controller combining both an absolute CoM and foot control objective, may yield exponential stability in the nominal case (foot in contact with firm ground), while becoming unstable if the contact is lost. We then presented the so-called Relative-CoM-to-Foot (RCF) controller that again yields exponential stability nominally, while preserving a passive and BIBO stable behavior even in case of a complete contact loss. The controller performance was validated in simulations, both for regulation and tracking cases.

[5]Remember: steady state: $z_R = -\frac{m_2 g}{k_R}$ in (64) for $w_2 = 0$ and $\ddot{z}_{R,ref} = 0$

[6]except for the case (as mentioned above) in which the controller from Sec. V-B uses equal CoM and foot damping and stiffness gains for which it is equivalent to the presented RCF controller, and thus remains stable.

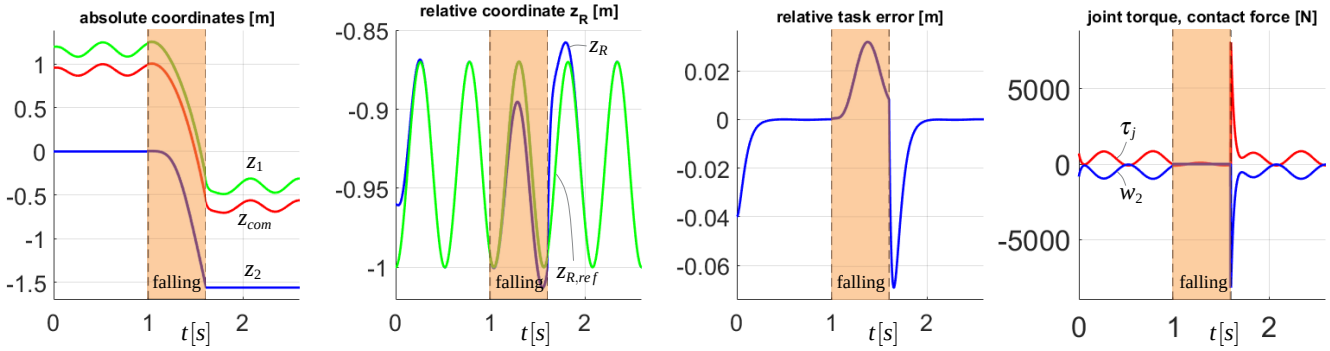

Fig. 3: Standing-falling-standing scenario: $z_{R,ref}$ following a sinusoidal reference.

REFERENCES

[1] Z. Vafa and S. Dubowsky, "The kinematics and dynamics of space manipulators: The virtual manipulator approach," *The International Journal of Robotics Research*, vol. 9, no. 4, pp. 3–21, 1990.

[2] E. Papadopoulos and S. Dubowsky, "Coordinated manipulator/spacecraft motion control for space robotic systems," in *Proceedings of 1991 IEEE International Conference on Robotics and Automation*, April 1991, pp. 1696–1701 vol.2.

[3] Y. Umetani and K. Yoshida, "Resolved motion rate control of space manipulators with generalized jacobian matrix," *IEEE Transactions on Robotics and Automation*, vol. 5, no. 3, pp. 303–314, Jun 1989.

[4] A. M. Giordano, G. Garofalo, and A. Albu-Schäffer, "Momentum dumping for space robots," in *2017 IEEE 56th Annual Conference on Decision and Control (CDC)*, Dec 2017, pp. 5243–5248.

[5] A. M. Giordano, D. Calzolari, and A. Albu-Schäffer, "Workspace fixation for free-floating space robot operations," in *2018 IEEE International Conference on Robotics and Automation (ICRA)*, May 2018.

[6] A. M. Giordano, C. Ott, and A. Albu-Schäffer, "Coordinated control of spacecraft's attitude and end-effector for space robots," *IEEE Robotics and Automation Letters*, vol. 4, no. 2, pp. 2108–2115, April 2019.

[7] S. Kajita, F. Kanehiro, K. Kaneko, K. Fujiwara, K. Harada, K. Yokoi, and H. Hirukawa, "Biped walking pattern generation by using preview control of zero-moment point," in *2003 IEEE International Conference on Robotics and Automation (Cat. No.03CH37422)*, 2003, pp. 1620–1626 vol.2.

[8] S. Lohmeier, T. Buschmann, and H. Ulbrich, "Humanoid robot lola," in *2009 IEEE International Conference on Robotics and Automation*, 2009, pp. 775–780.

[9] J. Urata, K. Nshiwaki, Y. Nakanishi, K. Okada, S. Kagami, and M. Inaba, "Online walking pattern generation for push recovery and minimum delay to commanded change of direction and speed," in *2012 IEEE/RSJ International Conference on Intelligent Robots and Systems*, 2012, pp. 3411–3416.

[10] J. Englsberger, A. Werner, C. Ott, B. Henze, M. A. Roa, G. Garofalo, R. Burger, A. Beyer, O. Eiberger, K. Schmid, and A. Albu-Schäffer, "Overview of the torque-controlled humanoid robot toro," in *IEEE-RAS Int. Conf. on Humanoid Robots*, 2014, pp. 916–923.

[11] C. Semini, N. G. Tsagarakis, E. Guglielmino, M. Focchi, F. Cannella, and D. G. Caldwell, "Design of hyq - a hydraulically and electrically actuated quadruped robot," *Proceedings of the Institution of Mechanical Engineers, Part I: Journal of Systems and Control Engineering*, vol. 225, no. 6, pp. 831–849, 2011.

[12] B. Henze, R. Balachandran, M. A. Roa-Garzon, C. Ott, and A. Albu-Schäffer, "Passivity analysis and control of humanoid robots on movable ground," *IEEE Robotics and Automation Letters*, vol. 3, no. 4, pp. 3457–3464, 2018.

[13] G. Mesesan, J. Englsberger, G. Garofalo, C. Ott, and A. Albu-Schäffer, "Dynamic walking on compliant and uneven terrain using dcm and passivity-based whole-body control," in *2019 IEEE-RAS 19th International Conference on Humanoid Robots (Humanoids)*, 2019, pp. 25–32.

[14] C. Dario Bellicoso, F. Jenelten, P. Fankhauser, C. Gehring, J. Hwangbo, and M. Hutter, "Dynamic locomotion and whole-body control for quadrupedal robots," in *2017 IEEE/RSJ International Conference on Intelligent Robots and Systems (IROS)*, 2017, pp. 3359–3365.

[15] M. Hutter, C. Gehring, D. Jud, A. Lauber, C. D. Bellicoso, V. Tsounis, J. Hwangbo, K. Bodie, P. Fankhauser, M. Bloesch, R. Diethelm, S. Bachmann, A. Melzer, and M. Hoepflinger, "Anymal - a highly mobile and dynamic quadrupedal robot," in *2016 IEEE/RSJ International Conference on Intelligent Robots and Systems (IROS)*, 2016, pp. 38–44.

[16] S. Fahmi, M. Focchi, A. Radulescu, G. Fink, V. Barasuol, and C. Semini, "Stance: Locomotion adaptation over soft terrain," *IEEE Transactions on Robotics*, vol. 36, no. 2, pp. 443–457, 2020.

[17] S. Feng, E. Whitman, X. Xinjilefu, and C. G. Atkeson, "Optimization based full body control for the atlas robot," in *2014 IEEE-RAS International Conference on Humanoid Robots*, 2014, pp. 120–127.

[18] M. A. Hopkins, D. W. Hong, and A. Leonessa, "Compliant locomotion using whole-body control and divergent component of motion tracking," in *2015 IEEE International Conference on Robotics and Automation (ICRA)*, 2015, pp. 5726–5733.

[19] M. Johnson, B. Shrewsbury, S. Bertrand, T. Wu, D. Duran, M. Floyd, P. Abeles, D. Stephen, N. Mertins, A. Lesman, J. Carff, W. Rifenburgh, P. Kaveti, W. Straatman, J. Smith, M. Griffioen, B. Layton, T. de Boer, T. Koolen, P. Neuhaus, and J. Pratt, "Team ihmc's lessons learned from the darpa robotics challenge trials," *Journal of Field Robotics*, vol. 32, no. 2, pp. 192–208, 2015.

[20] T. Koolen, S. Bertrand, G. Thomas, T. de Boer, T. Wu, J. Smith, J. Englsberger, and J. Pratt, "Design of a momentum-based control framework and application to the humanoid robot atlas," *International Journal of Humanoid Robotics*, vol. 13, no. 01, p. 1650007, 2016.

[21] S. Kuindersma, R. Deits, M. Fallon, A. Valenzuela, H. Dai, F. Permenter, T. Koolen, P. Marion, and R. Tedrake, "Optimization-based locomotion planning, estimation, and control design for the atlas humanoid robot," *Autonomous Robots*, vol. 40, no. 3, pp. 429–455, 2016.

[22] A. Herzog, N. Rotella, S. Mason, F. Grimminger, S. Schaal, and L. Righetti, "Momentum control with hierarchical inverse dynamics on a torque-controlled humanoid," *Autonomous Robots*, vol. 40, no. 3, pp. 473–, 2016.

[23] J. Englsberger, G. Mesesan, A. Werner, and C. Ott, "Torque-based dynamic walking - a long way from simulation to experiment," in *2018 IEEE International Conference on Robotics and Automation (ICRA)*, 2018, pp. 440–447.

[24] J. Englsberger, "Combining reduced dynamics models and whole-body control for agile humanoid locomotion," Dissertation, Technische Universität München, Munich, 2016.

[25] J. Englsberger, A. Dietrich, G. Mesesan, G. Garofalo, C. Ott, and A. Albu-Schäffer, "MPTC - Modular Passive Tracking Controller for stack of tasks based control frameworks," in *Proceedings of Robotics: Science and Systems*, Corvalis, Oregon, USA, July 2020.